Surface & Coatings Technology xxx (2016) xxx–xxx

Contents lists available at ScienceDirect

Surface & Coatings Technology

journal homepage: www.elsevier.com/locate/surfcoat

The application of photoluminescence piezospectroscopy for residual stresses measurement in thermally sprayed TBCs

C.R.C. Lima [a,b,*], S. Dosta [c], J.M. Guilemany [c], D.R. Clarke [b]

[a] Methodist University of Piracicaba, Rod. Luis Ometto, Km 24, Sta. Bárbara d'Oeste, SP, 13451-900, Brazil
[b] John A. Paulson School of Engineering and Applied Sciences, Harvard University, Cambridge, MA, USA
[c] Thermal Spray Center (CPT), University of Barcelona, C/Marti y Franqués, 1, Barcelona 08028, Spain

ARTICLE INFO

Article history:
Received 18 March 2016
Revised 16 July 2016
Accepted in revised form 28 July 2016
Available online xxxx

Keywords:
Photoluminescence piezospectroscopy
Residual stresses
Thermal barrier coating
Thermally grown oxide

ABSTRACT

Photoluminescence piezospectroscopy (PLPS) was used as a non-destructive technique for the measurement of residual stresses within the thermally grown oxide (TGO) layer beneath plasma-spray thermal barrier coatings (TBC). The technique has proved to be very effective for such measurements in YSZ thermal barrier coatings applied by EB-PVD but its application to thermal sprayed coatings has been hindered by optical scattering in plasma sprayed coatings of usual thicknesses. PLPS experiments were performed on TBCs with cold sprayed bond coatings and several different ceramic layer thicknesses after thermal cycling. The results are discussed as a function of the coating characteristics like bond coat spraying process, thickness of both bond and top coat, microstructural features, and damage accumulation.

1. Introduction

Thermal barrier coatings (TBC) are the best way to protect components of gas turbine engines and the demand for such coatings is becoming more important as higher temperature engines are being developed [1–3]. A TBC system generally consists of a ceramic top coat as a thermal insulator and a metallic bond coat (BC) on the underlying high-temperature alloy component [4,5]. The ceramic layer is normally 7–8% yttria partially stabilized zirconia (YSZ) [5–8] applied by atmospheric plasma spray (APS) or electron bean assisted physical vapor deposition (EB-PVD) [3,8]. The bond coat usually consists of either platinum modified nickel aluminide (Ni, Pt)Al (applied by electroplating and chemical vapor deposition – CVD) or a MCrAlY alloy, where M stands for Ni, Fe, Co or some combination of them. The alloys also usually include Hf, Ta or Re [8,10]. The main functions of the bond-coat alloy are to ensure good bonding between the high-temperature alloy component and the top coat as well as providing some oxidation and hot corrosion protection [4,5]. In use, a thin aluminum oxide scale forms on the bond-coat at its interface with the top-coat. The TBC lifetime often depends on the growth and internal stresses of this thermally grown oxide (TGO). Cracks nucleate at the thermally grown oxide and grow over the lifetime of the coating, eventually leading to the coating failure [8–11]. Actually, the failure of a TBC is a complex phenomenon that has instigated several research works. It has been accepted that cracks can start both in the TGO and in the YSZ close to the rough TGO mainly due to the complex stress state close to the rough YSZ/TGO/bond coat interface [12–14].

The formation of a dense and uniform α-Al_2O_3 scale is desirable due to its low oxygen diffusivity and low growth rate compared to other oxides. Other oxides, such as Cr and Ni oxides as well as spinels are undesirable due to their volume changes as they grow, and in the worst case can create protrusions contributing to the increase in local stresses and consequent failure [5,9]. The morphology, adherence and stresses in the TGO are very important issues in TBC evaluation and for life prediction. It has been observed that in EB-PVD TBC coatings, after a certain period of service life, the failure cracks typically follow the top coat/TGO interface. In a less extension, cracks can form at the "ridges" present on the bond coat surface before top-coat deposition [15]. For plasma sprayed TBC coatings, failure cracks propagate partly within the top coat (close to the TGO interface). It should be noted that even after coating general failure some adherent ceramic residues can be found [4,5,16–18].

Air plasma spray (APS), vacuum plasma spraying (VPS) and low-pressure plasma spray (LPPS) are the main techniques to apply bond coat onto superalloys [3,19]. These techniques provide fast manufacturing and a strong bonding with the part; but the main drawback is related to high temperatures that inevitably modify the coating microstructure by forming oxides. The oxide content is the principal problem for the aluminum depletion. It hinders the aluminum diffusion to the top of the BC, triggering the formation of Ni/Cr oxides and spinels in the TGO that are undesirable because of their volume change during formation. This volume change creates protrusions contributing to the increase of stresses and consequent failure. HVOF spraying has been

* Corresponding author at: Methodist University of Piracicaba, Rod. Luis Ometto, Km 24, Sta. Bárbara d'Oeste, SP, 13451-900, Brazil.
E-mail address: crclima@unimep.br (C.R.C. Lima).

http://dx.doi.org/10.1016/j.surfcoat.2016.07.084
0257-8972/

more recently used as an alternative deposition method because of its low cost and high quality deposits, which have oxidation rates at high temperature at the same level or even lower than those of similar VPS or LPPS coatings [11,17,18]. With this low oxidation perspective, some recent studies have investigated metallic bond coats formed by cold gas spray (CGS) [19,20].

In contrast to the more traditional coating methods, cold gas spray (CGS) utilizes the kinetic energy of the particles in a supersonic flow to deposit an adherent coating as a result of the severe plastic deformation produced when the particles impact the surface. The main advantages of CGS over conventional thermal spray techniques are related to the absence of thermal energy so there is no grain growth and no particle surface oxidation. As a result, a coating almost free of any oxides is obtained, allowing more free aluminum for diffusion to the surface to form the protective α-Al_2O_3 TGO layer on subsequent high-temperature exposure. As a result, CGS is increasingly being recognized as an alternative for the manufacturing of bond coats for thermal barrier coatings [20,21].

In the search of better understanding and control of the residual stresses leading to the failure of a TBC, several measurement techniques have been adopted. These include X-ray diffraction (XRD) and layer removal methods, among others [22–25]. Photoluminescence piezospectroscopy (PLPS) is a non-destructive technique for the measurement of residual stresses within the thermally grown oxide (TGO), including when formed underneath a ceramic top-coat (TBC) [26]. The technique has proven to be very effective for such measurements in YSZ thermal barrier coatings applied by EB-PVD [26–28]. Its application for thermal sprayed coatings is still not solved since the resulting lamellar structure is said to spread the laser beam then weakening the resulting photoluminescence signals [29]. The piezospectroscopic technique is an optical method that utilizes the luminescence from trace Cr^{3+} dopants incorporated into the aluminum oxide formed by oxidation. The spectrum of aluminum oxide consists of two characteristic R-lines, R1 and R2, due to electronic transitions in Cr impurities. The luminescence is excited by a laser beam with an energy selected to penetrate through the zirconia TBC and still be within the optical absorption band of chromium-doped aluminum oxide [30]. If the oxide is stressed, the frequency of the Cr^{3+} luminescence shifts from its stress-free value, the piezospectroscopic effect. The frequency shift is related to the stress by a general equation and measuring this shift the biaxial stresses can be obtained after some calculation [30].

The objective of this work was to assess residual stresses in TGOs formed on thermally sprayed TBCs with cold sprayed bond coats by PLPS experiments. Optimization of the PLPS data collection parameters was employed to overcome limitation reported in previous works related to scattering issues in plasma sprayed TBC. The results are discussed as a function of the PLPS process parameters, coating thickness and number of thermal cycles.

2. Experimental procedure

The metallic coatings were applied onto Inconel 625 Ni-based superalloy (25 × 20 × 5 mm) specimens. One half of the surface area (25 × 10 mm)was coated with the YSZ coating and the other half was left without any YSZ coating as shown in Fig. 1. Metallic plates were used to protect the substrate (half part) for ceramic spraying. The feedstock bond coat powder was an experimental gas atomized NiCrAlY powder (AE10086, Oerlikon Metco) with composition Co32Ni21Cr8Al0.5Y, a spherical morphology, and a particle size of 35 + 11 μm. The ceramic powder was a commercial YSZ (203 NS - Oerlikon Metco) spray-dried, with spherical morphology, and a particle size of −125 + 11 μm.

Before spraying, all alloy substrates were degreased with acetone and grit blasted with white corundum, using a pressure of 5.6 bar, 45° incidence angle, and blasting distance of 250 mm. The grit blasted surface roughness was 4.5 μm (Ra). The samples were placed in a circular sample holder and were simultaneously sprayed for every material

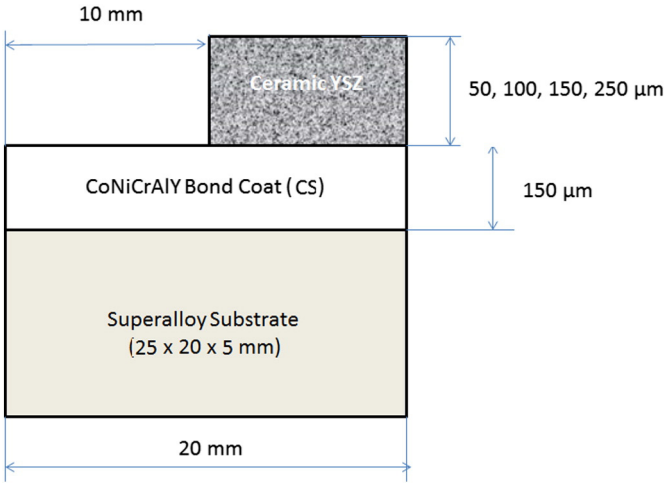

Fig. 1. Scheme of the test specimen.

(bond and top coat) with a rotational speed of 500 mm/s at the substrate surface. Cooling with air jet to sample back side was applied during ceramic deposition.

The morphology of the metallic powders used to form the bond coat is shown in Fig. 2. The chemical compositions of the metallic and ceramic powders are shown in Table 1.

The bond coats were deposited using a Kinetiks® 4000 cold gas spray system (CGT GmbH), with a maximum operating pressure of 40 bar and nitrogen as the propellant gas. A F4-MB plasma spray gun (Plasma Technik, Sulzer Metco, Westbury, USA) was used to apply the ceramic top coats. The thermal spraying parameters used for metallic and ceramic coatings application are shown in Table 2. The bond coat was 150 μm thick whereas four different ceramic top coating thicknesses were prepared: 50, 100, 150 and 250 μm.

Laser Scattering (Microtrac SRA150), Scanning Electron Microscopy (SEM: JEOL JXA840) and flow rate test (ASTM B-213-90) were used for powder particle size distribution and for general powder characterization. XRD (Siemens D-500, Cu Kα = 1.5418 Å, 40KV, 30 mA) was applied to reveal phase content of the starting powder. As sprayed coatings characterization included cross-sectional Optical Microscopy (OM-Leica DMI5000 M) and Scanning Electron Microscopy (JEOL - JXA840), as well as phase analysis by Energy Dispersive Spectroscopy-EDS (Quantum, Kevex). For TGO and thermal cycled coating microstructure analysis, a ZEISS - ULTRA 55 scanning electron microscope was employed. Coating surface roughness was measured in an Olympus

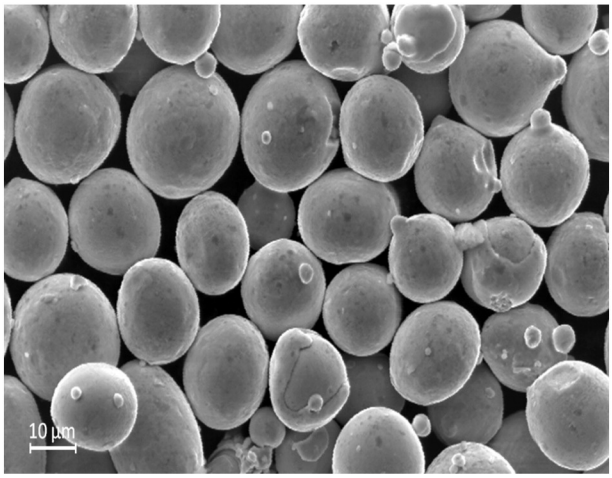

Fig. 2. SEM images of the new CoNiCrAlY powder.

Please cite this article as: C.R.C. Lima, et al., Surf. Coat. Technol. (2016), http://dx.doi.org/10.1016/j.surfcoat.2016.07.084

Table 1
Chemical composition of the materials used in the experiments (wt%).

Material	Co	Ni	Cr	Al	Y	Mo	Fe (max)	Nb + Ta	ZrO_2	Y_2O_3	Other (max)
Inconel 625	–	Bal.	20–23	–	–	8–10	5–11	3.1–4.1	–	–	–
CoNiCrAlY	Bal.	29–35	18–24	5–11	0.1–0.8	–	–	–	–	–	1.0
YSZ 203 NS	–	–	–	–	–	–	–	–	92	8	–

Table 2
General thermal spraying parameters.

CGS	p (bar)	T (°C)	Nozzle type	v (mm/s)	Powder Feed Rate (Kg/h)	Passes	Pass Spacing (mm)	SOD (mm)
CoNiCrAlY	50	1000	24 WC	550	2	1	1	20
APS	Ar Flow Rate (l/min)	H_2 Flow Rate (l/min)	Amperage (A)	Voltage (V)	Powder Feed Rate (Kg/h)	Passes	Pass Spacing (mm)	SOD (mm)
ZrO_2-8%Y_2O_3	40	12	630	68	0,9	20	5	120

SOD = Standoff Distance; v = Particle Velocity

LEXT Confocal Microscope - OLS 4000. Values quoted for roughness are an average of 20 measurements for each coating.

Thermal Cycling was accomplished in an automatic system, controlled using LabView software (National Instruments), using a Thermo-Scientific Lindberg Blue M tube furnace. The thermal cycling is shown in Fig. 3. The thermal cycles consisted of a 15 min period at 1121 °C in air environment, followed by cooling to 200 °C in ambient air. Sets of samples were systematically extracted from the holder for PLPS experiments after 50, 100, 200, 300, 400, 500 cycles as well as after the end of life, determined as the time at which the spalled area reached 40% of the total coated area. After residual stress measurements, some selected samples were metalographically prepared to be observed by SEM. The thermal grown oxide (TGO) layer was then measured and analyzed regarding to exposition times and ceramic coating thickness.

The measurements of residual stresses were carried out by Cr^{3+} photoluminescence piezospectroscopy (PLPS) using a Horiba LabRAM ARAMIS system. The excitation source was a green Ar ion laser with a photon wavelength of 514 nm and nominal power of 30 mW. The spectra were typically obtained using a 10% power (Filter D-1) and making ten successive spectral acquisition times of 5 s each. The laser beam was focused perpendicular to the surface of the coating, and mapping a crossing line of at least 400 μm long on the specimen surface. The confocal hole aperture was 400 μm and the slit aperture width was 20 μm. A 10× objective lens collected the light scattered from the specimen and was analyzed using a 1800 lines per mm grating. The R2 peak shift, relative to a ruby standard, was used for stress calculation. Air conditioning unit was used to maintain the room temperature at 22 °C for all the PLPS measurements because of the temperature dependence of frequency of the R1 and R2 peaks. Peak fitting and deconvolution was performed with NGS LabSpec 5 software. A total of at least 40 individual measurements were averaged for residual stress level computation. Residual stress calculation followed the equation for biaxial stresses given by:

$$\overline{\Delta v} = \frac{2}{3}\prod ii\ \overline{\sigma} \tag{1}$$

where the piezospectroscopic tensor $\prod_{ii}$ is 7.60 cm^{-1}/GPa [27].

3. Results and discussion

3.1. Coatings structural characterization

Representative images of the TBC coating systems are shown in Fig. 4 for the different coating thicknesses. The general microstructure of the

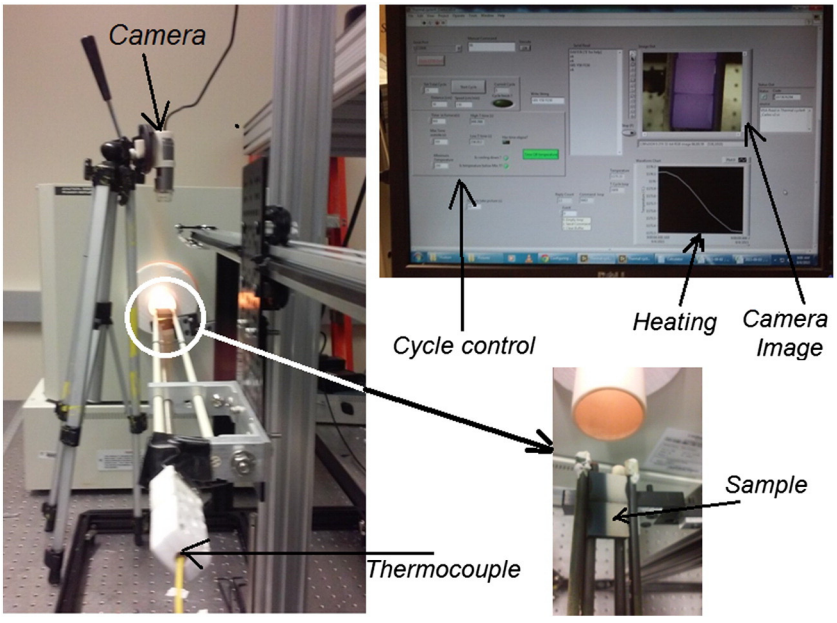

Fig. 3. Thermal cycling equipment developed at Harvard University.

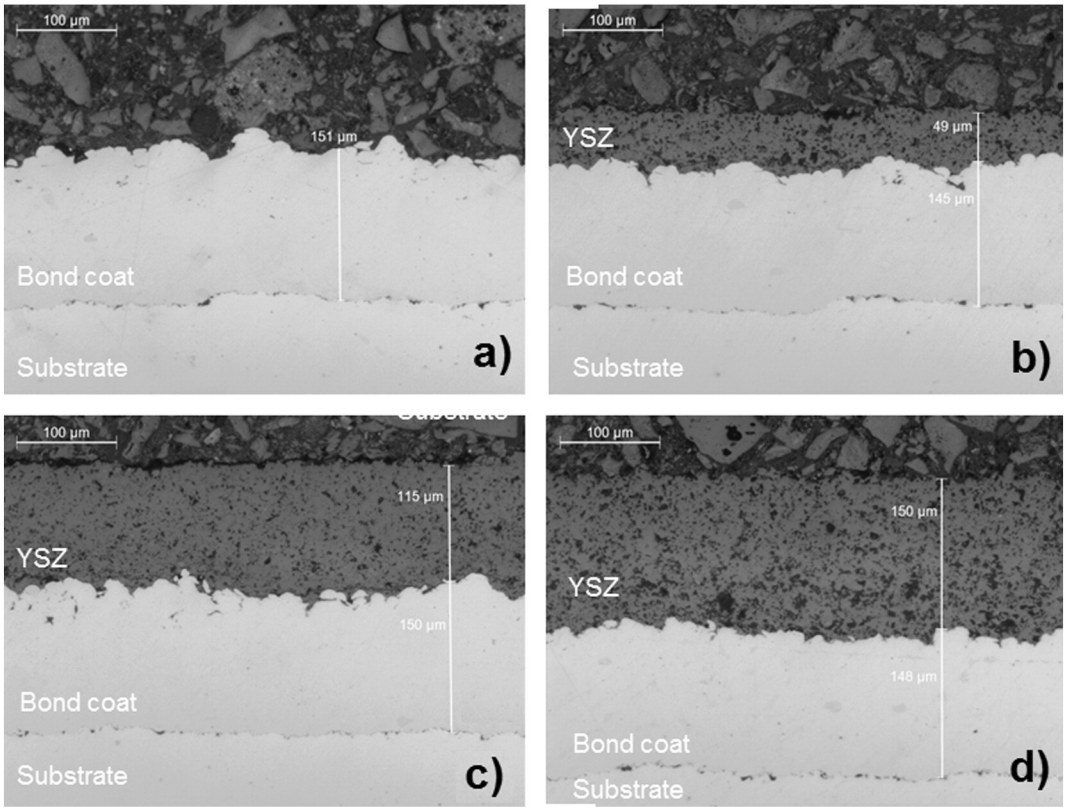

Fig. 4. Optical cross sectional images of a) the bond coat without top coat, and a TBC coating system with b) 50, c) 100, and d) 150 μm thick ceramic over a 150 μm bond coat.

coatings was practically identical for all the systems. Further and complementary data on the general characteristics of the YSZ TBC with a cold sprayed bond coat using the new CoNiCrAlY powder (AE10086) can be found elsewhere [31].

The roughness of the as sprayed bond coat was measured as 3.8 μm (Ra). The grit blasted substrate had a roughness of 4.5 μm, indicating just a slight reduction in surface roughness after bond coating, probably related to surface smoothing by filling the concave regions. A more intense decreasing in roughness was observed for the roughness of the thermal cycled TBC coating surfaces that varied from 3.7 μm for the as sprayed TBC with 50 μm ceramic top coat to 2.0 μm for the same TBC after 200 thermal cycles. In this case, the decreasing in roughness is probably due to surface degradation by removal of debonded particles. The morphology and residual stress in the TGO scale may vary depending on the roughness of the bond coat surface prior to oxidation. Rough surfaces result in lower R2 frequency shifts due to tensile contributions of the stress over convex prominences of the surface. Since the bond coat was the same for all TBC coatings, and did not vary after the ceramic top coat application, no further roughness influence in the comparative residual stress measurement was taken into account.

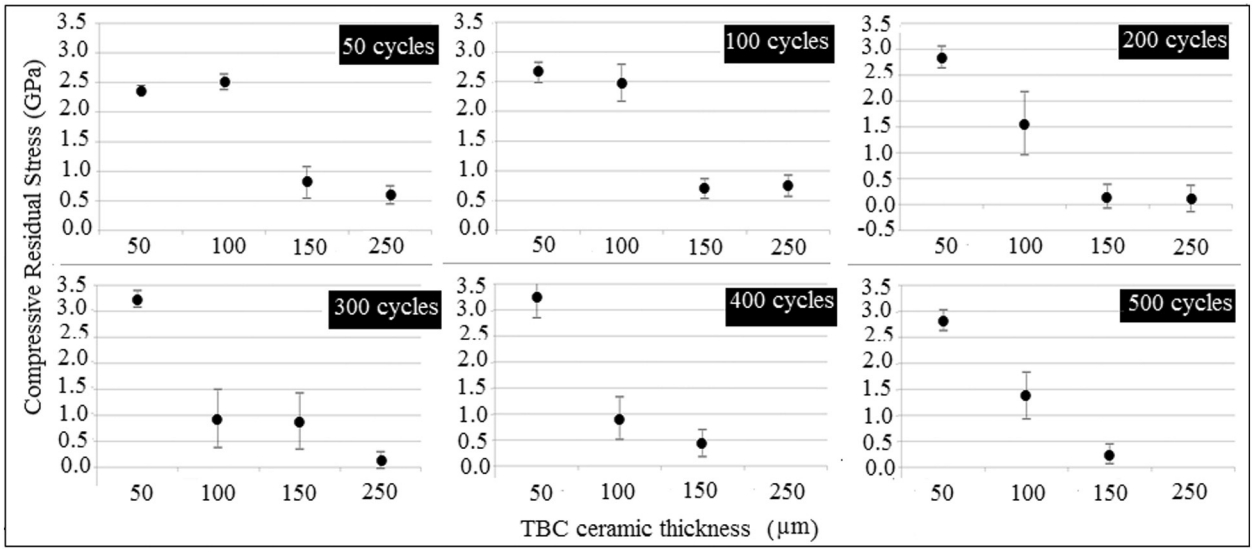

Fig. 5. Compressive residual stresses measured after 50 through 500 thermal cycles.

Please cite this article as: C.R.C. Lima, et al., Surf. Coat. Technol. (2016), http://dx.doi.org/10.1016/j.surfcoat.2016.07.084

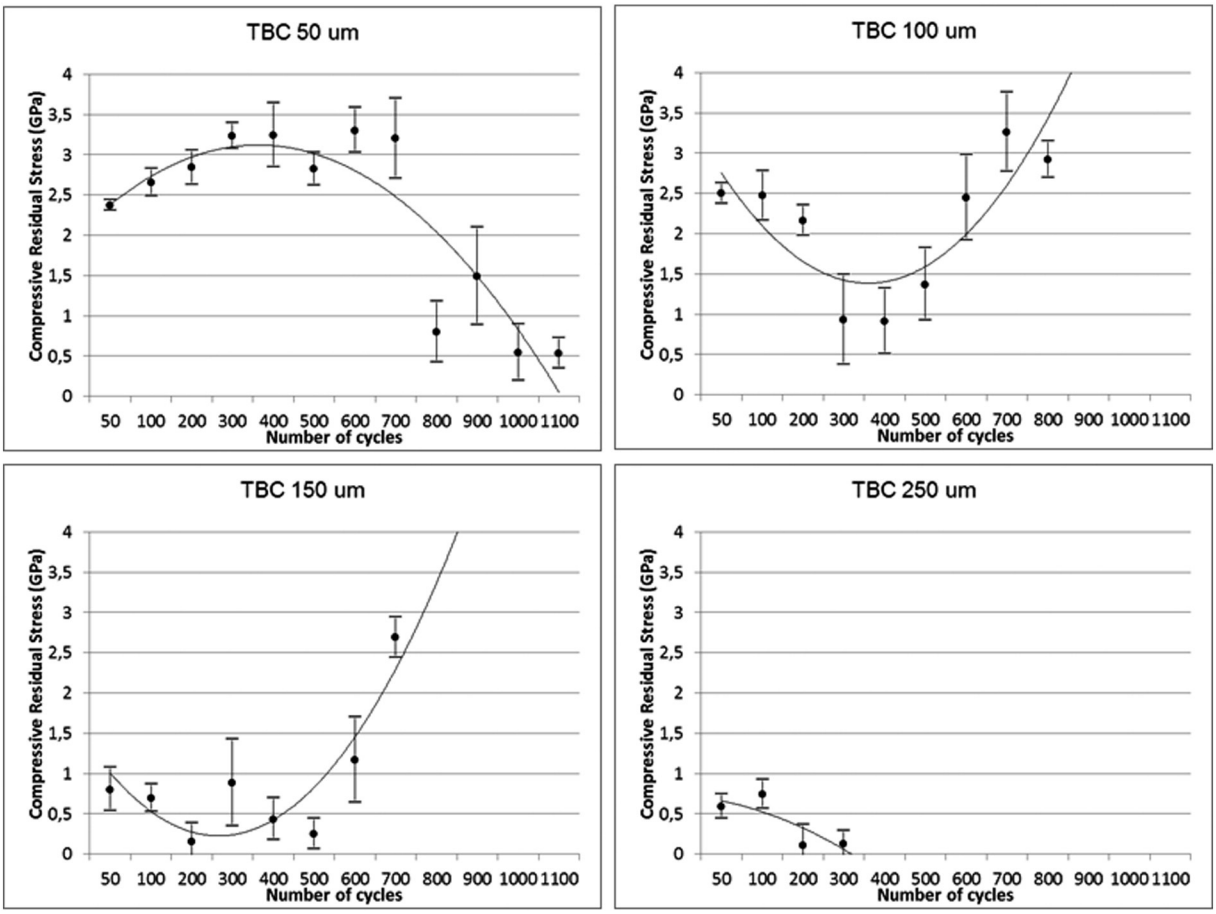

Fig. 6. Residual stresses for the different thicknesses of ceramic coatings after thermal cycling at 1121 °C. The last results in each graphic correspond to the failure of the coating. The lines through the data points represent a general tendency of residual stress with increasing number of cycles using a polynomial fitting. The values shown are the average of measurements recorded at 40 different locations.

3.2. Residual stress measurements

The PLPS measurements were initially carried out on the as-sprayed TBCs. No luminescence signals were observed meaning that no alumina was detectable before thermal cycling. After thermal cycling, strong R1 and R2 peaks characteristic of alumina were detectable. Furthermore, the frequencies of the R2 lines were dependent on the number of cycles and the different coating thicknesses. These findings, plotted in terms of the compressive residual stresses in the TGO are presented in Fig. 5 after 50 through 500 thermal cycles.

It is worth to mention that in the present experiments with the appropriate equipment calibration and set-up it was possible to get correct luminescence signal regardless of the ceramic coating thickness, then allowing the residual stress calculation. The main parameters to be adjusted are the laser power and the combination of exposure time and accumulation number. The intensity of the resulting signal varies but this fact by no means compromises the peak shift evaluation. All data-acquisition conditions were maintained constant for all specimens.

Except for the TBCs with the thinnest, 50 μm, ceramic top-coat, which shows an increase of the compressive stresses until 400 cycles,

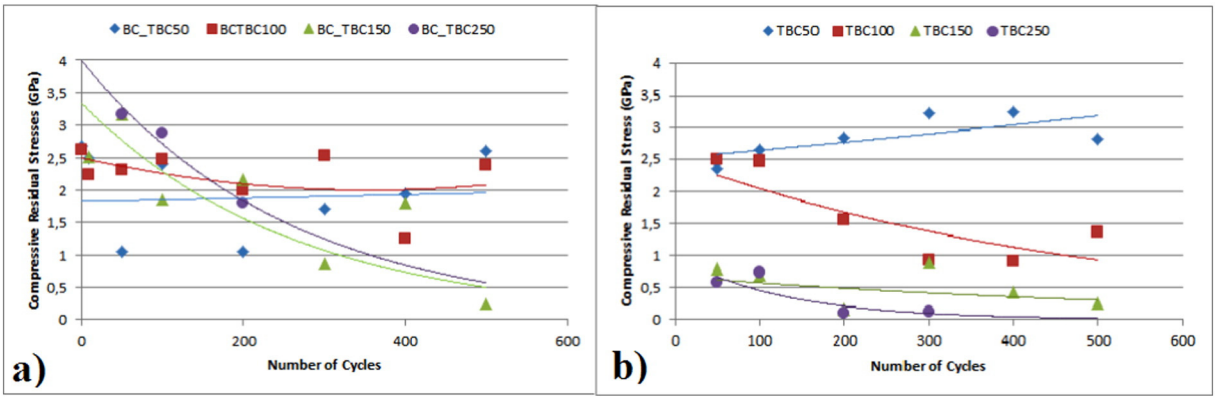

Fig. 7. Average residual stresses for a) the bond coats with no top coat, and b) the different thicknesses of ceramic coatings after thermal cycling at 1121 °C. Data points are the average of 40 individual measurements in different locations.

Please cite this article as: C.R.C. Lima, et al., Surf. Coat. Technol. (2016), http://dx.doi.org/10.1016/j.surfcoat.2016.07.084

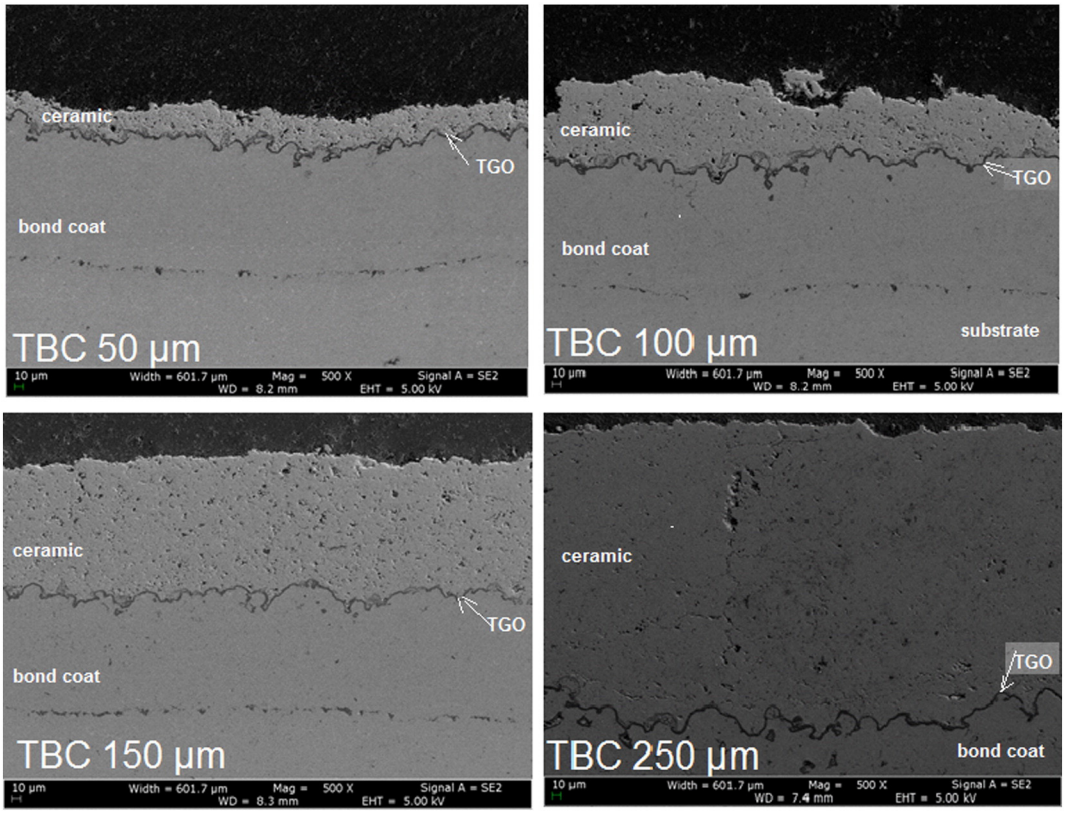

Fig. 8. SEM cross sections of the coatings after 50 thermal cycles.

there is a general tendency of the compressive stress to decrease with increasing number of thermal cycles until 500 cycles. The TBC with a 100 µm ceramic coatings showed the highest scattering of results. The highest stresses are for the TBC with a ceramic thickness of 50 µm that reaches 3.64 GPa after 400 cycles. For the TBCs with a ceramic thickness of 150 and 250 µm, a much lower level of residual stress is shown until 500 cycles, between 0 and 1 GPa, including some tensile stresses after 200 cycles. The scattering of results is mainly attributed to the influence of TGO roughness since the highly undulating nature of TGO/BC interface gives rise to out of plane tension.

For the thicker TBCs, increasing thermal cycling, after 500 cycles, there is a change in the decrease trend then showing an increase propensity to higher compressive stresses for the thicker coatings until the coating failure. The coating failure was defined as the spalling or detachment of more than 40% of the coated area. These general trends of the residual stresses for the four different TBC coatings are shown in the graphs of Fig. 6.

The mentioned trend was not observed only for the thinner coating (50 µm) that, after an initial increasing below 400 cycles, has shown a general tendency of reduction in the residual stresses until complete failure after 1100 cycles. For the 250 µm ceramic coated TBC the premature failure just after 300 cycles did not allow to evaluate that trend. But according to the results for TBC 100 and TBC 150 µm, the same tendency could be foreseen. Fig. 7 shows the average general behavior for the evolution of residual stresses in the bond coats with no ceramic top coat, measured on the half part of each coating sample, as well as the evolution for the TBC full coated ceramic samples until 500 thermal cycles. Despite the differences in the stress level, a similar tendency for both samples, with or without a ceramic top coat, can be seen. The lower stress values for the bond coat with no ceramic top coat are credited to the fact that there is no constraint from the top coat, and furthermore, some oxide scale spallation is seen to occur after thermal cycling. The stress increasing tendency of the thicker ceramic coatings (Fig. 6) when cycling longer than 500 cycles could be explained by the change in the area probed by the laser on the thermal cycled samples as the samples already presented some coating degradation and PLPS was performed on the apparently intact regions of the coatings. This point will be better discussed in the discussion section.

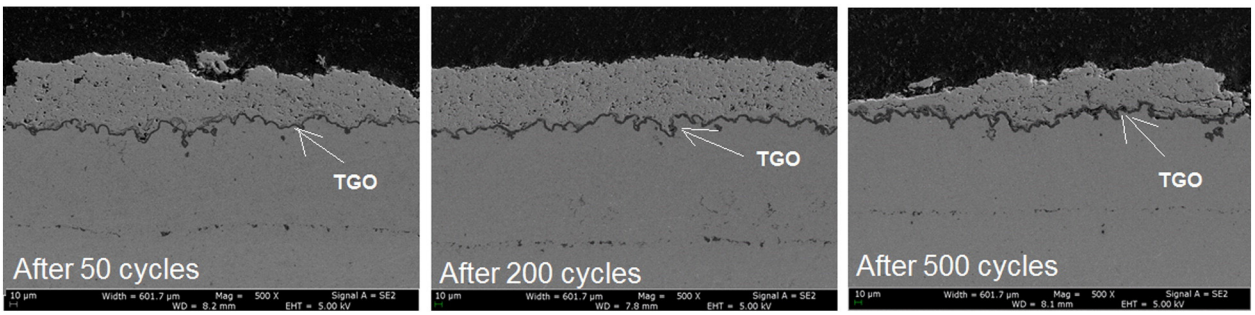

Fig. 9. SEM cross section of the 100 µm TBC after thermal cycling.

Please cite this article as: C.R.C. Lima, et al., Surf. Coat. Technol. (2016), http://dx.doi.org/10.1016/j.surfcoat.2016.07.084

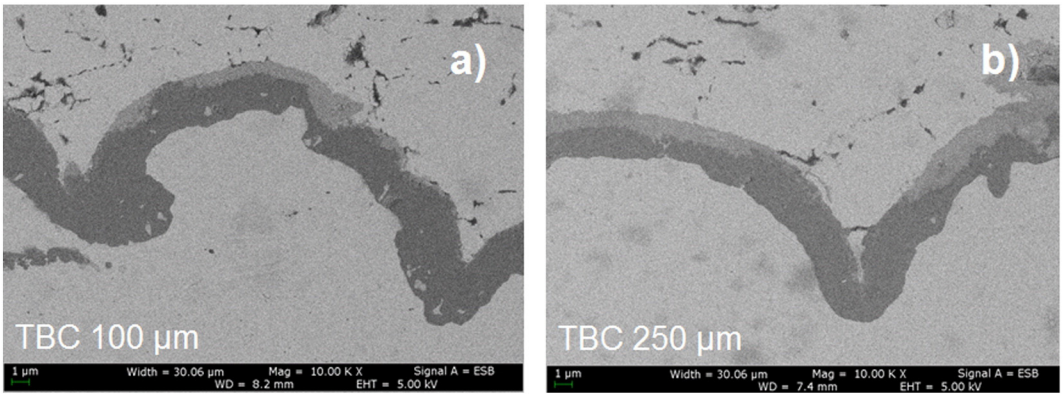

Fig. 10. SEM cross sectional image of thermally grown oxide formed after 50 thermal cycles for: a) a 100 µm ceramic top-coat; b) 250 µm ceramic top-coat.

3.3. TGO characteristics and evolution

The cross sections of the coatings after 50 thermal cycles are shown in Fig. 8. A similar thickness of the TGO formed for the four different coating thicknesses can be reported. The wrinkling of the TGO profile can be observed and is very similar for all the coatings.

A similar aspect of the TGO was observed after additional thermal cycling, with no relevant changes in TGO growing and oxides formation for all coatings as exemplified in Fig. 9 that shows the TGO aspect after additional thermal cycling for the TBC with 100 µm ceramic layer until 500 cycles. As a matter of fact, when increasing thermal cycling, an increasing in the formation of a second phase (light grey) that differs from the α-Al_2O_3 (dark grey phase) is observed. It should be emphasized that no significant changes were noted in the thickness of the TGO formed regardless of the TBC thickness or number of cycles until 500 thermal cycles. This is evidenced when comparing the TGO of a TBC with 100 or 250 µm of ceramic after 50 thermal cycles (Fig. 10) as well as for the different TBC thicknesses after 200 cycles (Fig. 11) with a similar TGO thickness around 4 µm. Diverse values of TGO thicknesses have been reported by other authors mainly due to differences in heating or thermal cycling procedures and parameters, coating materials and thicknesses, application processes, measurement procedure among others. Focusing just on thermally sprayed TBCs, Rabiei and Evans [32] measured TGO from 3.5 to 7 µm thick after thermal cycling from 216 to 1944 h at 1010 °C. Wang et al. [33] reported a TGO ranging from 2 to 8 µm for air plasma sprayed TBC exposed to 1200 °C for different times. A TGO thickness varying from 2 to 6 µm is reported by Martena et al. [34] from isothermal treatment of TBC at 1070 °C.

The maximum measured thickness was 5 µm for the 100 µm TBC, with an evolution of just 1 µm in thickness from 200 to 500 thermal cycles, as evidenced in Fig. 12. EDS measurements have shown that the TGO formed is mainly α-Al_2O_3 (dark grey phase in Figs. 10 to 12), as expected, and a second phase (light grey) mainly constituted of Cr, and Ni, most probably as NiO, Cr_2O_3 or spinel-type oxides. Alumina is the preferred oxide because it forms a continuous scale, with slow growth rate and a superior adherence to BC. There are different assumptions in the literature about the alumina scale growth. Some suggest that alumina scale grows preferentially by outward aluminum diffusion, others support that scale growth occurs by inward oxygen diffusion, and some state that the growth occurred by both cation and anion transport in the alumina scale [35,36]. Some studies have stated that Al_2O_3 would form first in CoNiCrAlY bond coats during thermal exposure in air [37]. But, according to more recent studies, it was found that the upper part of the TGO after 50 and 200 thermal cycles at 1050 °C consisted of a chromia + spinel layer and of mixed oxide clusters, other than the Al_2O_3 [38]. The same typical oxide composition is found in this research. A possible explanation for that is the compositional inhomogeneity in the thermally sprayed TBC systems that could promote the preferential formation of $(Cr,Al)_2O_3$, NiO and other oxides at the first stage of oxidation. Complimentarily, it might also be possible that the early formation of mixed oxides is due to the lack of properly developed beta-phase at the beginning of thermal cycling.

3.4. Discussion

As observed by several authors [32,34,38], the failure of TBCs in thermal cycling is caused by the crack propagation in the YSZ coating next to and along the YSZ/bond coat interface. The failure occurs through the nucleation and growth of discontinuities, which is assisted by the crack nucleation and propagation related to the stresses generated by the TGO. The residual stresses that lead to cracking occur from a combination of macro and micro effects that include coefficient of thermal expansion (CTE) mismatch between the coating and substrate and the differential thermal expansion coefficients between different phases present in the coating. The stresses across the TGO close to the bond coat are higher than close to the ceramic, and the stresses at thickness imperfections in the TGO are smaller than in the regular TGO near the bond coat [39]. It is normally accepted that TBC failure can occur

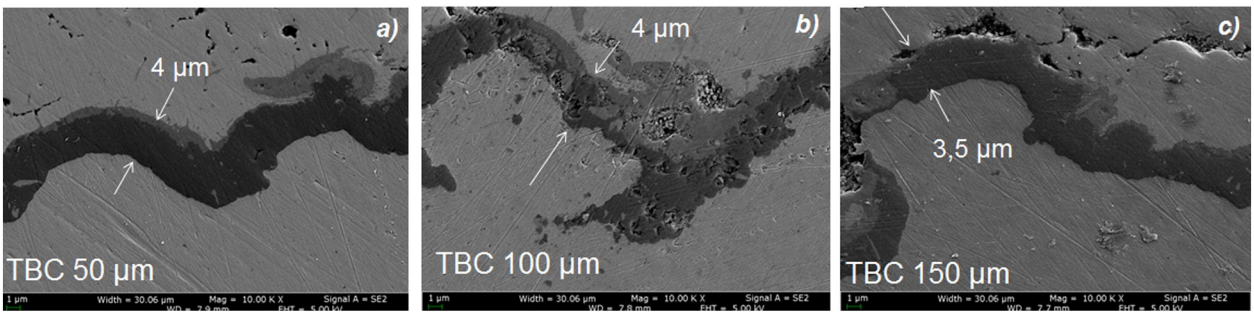

Fig. 11. SEM cross sectional image of the TGO thickness for different TBC thicknesses after 200 thermal cycles: a) 50 µm; b) 100 µm; c) 150 µm.

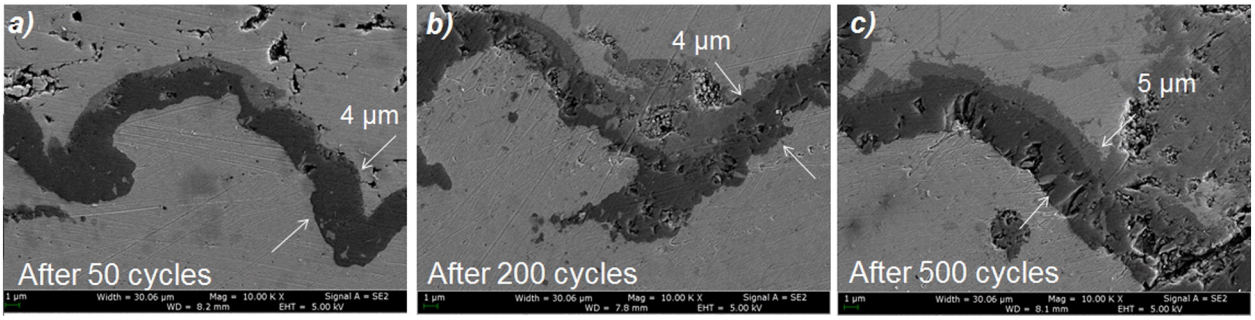

Fig. 12. SEM cross sectional image of the TGO thickness for 100 μm TBC after a) 50; b) 200; and c) 500 thermal cycles.

when the TGO growth exceeds a critical thickness. The mechanics of this form of failure are similar to the origin of a critical thickness for the loss of coherence of epitaxial thin films, specifically when the release of stored elastic strain energy in the growing film exceeds the fracture resistance [40].

To investigate the second phase present in the TGO, EDS was performed onto the TGO of a 100 μm TBC focusing the region with dark grey α-alumina and light grey mixed oxides. As can be seen in the details of Fig. 13, the lighter phase is mainly constituted of Cr, Co and Ni oxide what could justify the systematic reduction in the general residual stress for the thicker coatings (Fig.5) as that second phase is increasingly observed when increasing ceramic thickness in the TBC until 500 cycles.

Some mechanics modeling indicates that the TGO should ideally remain elastic to the highest temperatures and not creep to prevent rumpling on thermal cycling that can lead to the development of local separations at the TBC interface [41] what is the case for α-alumina TGO. However, rumpling is known to commonly occur on thermal cycling and, additionally, as thermal exposure further proceeds, the initially formed Al_2O_3 transforms to chromia + spinel and other detrimental oxides that results in increased cracking associated with the TGO and then longer cracks within the ceramic/bond coat interface. These oxides with low mechanical integrity are more susceptible to crack nucleation and propagation as discussed by Chen et al. [38] then resulting in lower residual stresses when sampling volumes with a high incidence of these oxides.

With further thermal cycling after 500 cycles, the failure is believed to be driven by subsequent cracking propagation at the ceramic top coat which seems more accentuated for thicker coatings as thermal cycling proceeds. The explanation for the increasing residual stress tendency (Fig. 6) for the thicker TBCs (100, 150 and 250 μm) is proposed to be related to the coating volume probed by the laser in PLPs since a visually undamaged region (with thicker TGO) was chosen for the measurements after 500 cycles. It should be remembered that coating failure was defined as the collapse of more than 40% of the coating surface

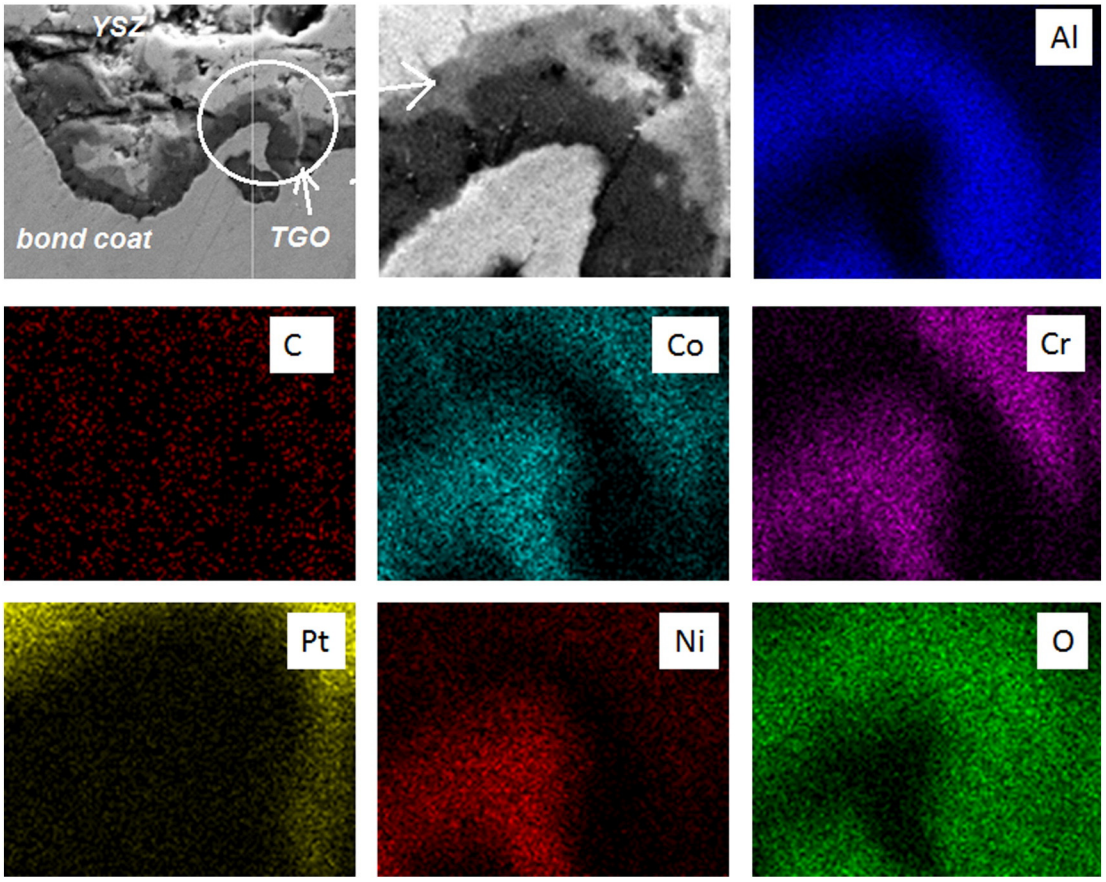

Fig. 13. EDS results from the cross section of a 250 μm TBC after 50 thermal cycles at 1121 °C for 15 min. The SEM image shows the second phase formed over the α-Al_2O_3 TGO scale.

Please cite this article as: C.R.C. Lima, et al., Surf. Coat. Technol. (2016), http://dx.doi.org/10.1016/j.surfcoat.2016.07.084

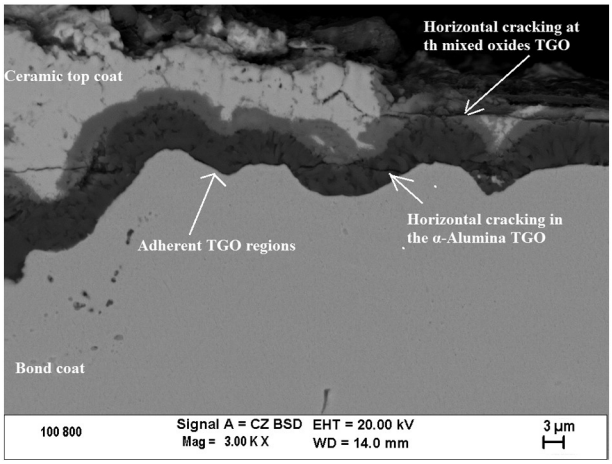

Fig. 14. Backscattered SEM images of 100 µm TBC at failure after 800 thermal cycles at 1121 °C for 15 min showing the presence of TGO scale regions that are still adherent. These regions when probed by PLPS might explain the high residual stresses values measured.

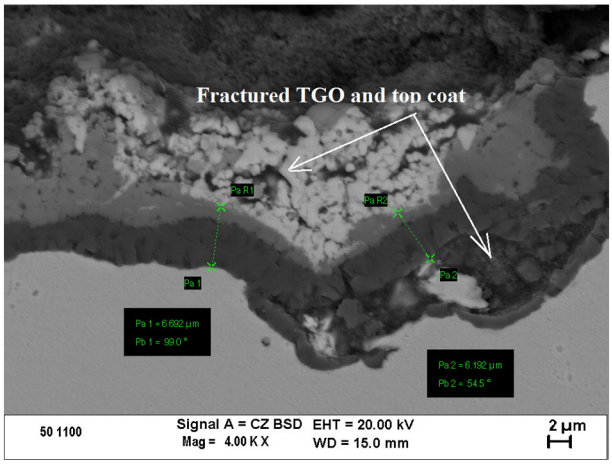

Fig. 16. Backscattered SEM images of a 50 µm TBC failed after 1100 thermal cycles at 1121 °C for 15 min showing damaged TGO scale as well as top coat fracture and collapse. Note that the TGO has reached around 7 µm of thickness.

area. Then, before final failure, some mixed regions of the TGO were probed, i.e. completely adherent regions and detached regions of the TGO, as can be observed in Fig. 14 that was got from a failed sample after 800 thermal cycles.

Differently, the tendency of the thinner TBC coating (50 µm) until 500 cycles is to increase with prolonged cycling (Fig.7). This is in a good agreement with previous works both in the increasing tendency and in the stress values measured taking into account the differences in thermal cycling dwell time [27,42,43]. It should be noted that the same tendency is observed for the bond coat alone (Fig. 7) but the stress values are lower since there is no constraint from the top coat and oxide scale spallation is present as can be observed in Fig. 15 from a bond coat alone after 200 cycles. From 500 cycles to final failure at 1100 cycles the decreasing tendency in residual stress of the thinner TBC (Fig. 6) is credited to general coating cracking both in the thin top coat and in the TGO leading to coating collapse, as shown in Fig. 16. Note that the TGO is considerably thicker than at 500 cycles.

From the previous discussion and considering the present results, it should be pointed out that the photoluminescence piezospectroscopy can be consistently used to measure TGO residual stresses of plasma sprayed thermal barrier coatings until 250 µm even considering the attenuation of photoluminescence signal. PLPS can be useful to predict

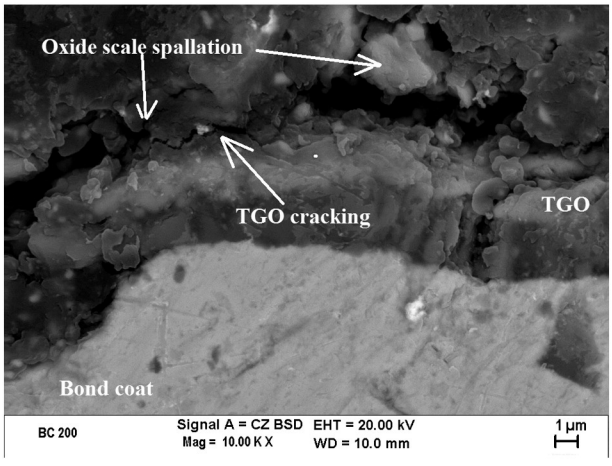

Fig. 15. Backscattered SEM images of a bond coated superalloy with no ceramic top coat after 200 thermal cycles at 1121 °C for 15 min showing the presence of TGO scale with cracking. Measured stress values are low compared to top coated samples since there is no constraint from the top coat and oxide scale spallation is evident.

TBC life. It can be also suggested that the inflection point of the stress changing tendency, as pointed in Fig. 6, means that the general coating has already failed but there are still some adherent and almost intact regions of the coating that are still effective in the substrate protection.

4. Conclusions

TBC coatings with different ceramic layer thicknesses were tested by Cr^{3+} photoluminescence piezospectroscopy to evaluate the residual stresses at the thermally grown oxide formed after thermal cycling at 1121 °C. Scanning Electron and Optical Microscopy helped in the TGO and coating structure evaluation. The results can be summarized as follows:

- A new CoNiCrAlY powder (AE10086) with composition Co32Ni21Cr8Al0.5Y was deposited onto Inconel 615 substrates by cold spray as a bond coat for an YSZ TBC. The coatings presented a very homogeneous and dense microstructure with a lower surface roughness as compared to the grit blasted substrate
- Photoluminescence piezospectroscopy was effective for residual stress measurements at TGO formed on cold sprayed bond coat of air plasma sprayed TBCs with ceramic layer thickness varying from 50 to 250 µm and proved to be indicated as a non-destructive tool for coating quality and failure control.
- Similar TGO thicknesses, around 4 µm, were found by SEM imaging after additional thermal cycling in the range of the experimental approach until 500 thermal cycles. Beyond that TGO thickens and got around 7 µm for the 50 µm TBC after 1100 cycles.
- According to the results, residual compressive stresses measured in the TGO were found to be around 2.5 GPa after 50 fifteen-minute cycles at 1121 °C for the thinner coatings, then decreasing for the thicker coatings. The highest stresses are for the TBC with a ceramic thickness of 50 µm that reaches 3.64 GPa after 400 cycles.
- Until 500 cycles, the 50 µm coating shows an increasing residual stress tendency when increasing the number of thermal cycles that agrees with the results for a bond coated substrate without ceramic top coat. For thicker coatings a general tendency of compressive stress reduction is observed as the coating thickness increases. This trend changes with further thermal cycling until coating final failure.
- The decreasing of compressive stress for thicker coatings until 500 cycles is credited to the extensive formation of a second phase in the TGO mainly constituted of Cr, Co and Ni oxides that are detrimental oxides resulting in increased cracking associated with the TGO and then longer cracks within the ceramic/bond coat interface. These oxides with low mechanical integrity are more susceptible to crack

nucleation and propagation then resulting in lower residual stresses when sampling volumes with a high incidence of these oxides.

Acknowledgments

The authors would like to thank the technical help from Mary Gurak, Samuel Shian, and Peter Kjeer at SEAS, Harvard University, and Victor Crespo at CPT, University of Barcelona.

This study was conducted with support from CNPq (203809/2014-9) Brazil.

References

[1] C.U. Hardwicke, Y.C. Lau, Advances in thermal spray coatings for gas turbines and energy generation: a review, J. Therm. Spray Technol. 22 (5) (2013) 564–576.
[2] A.G. Evans, D.R. Mumm, J.W. Hutchinson, G.H. Meier, F.S. Pettit, Mechanisms controlling the durability of thermal barrier coatings, Prog. Mater. Sci. 46 (2001) 505–553.
[3] R.N. Katz, Thermal barrier coatings beat the heat, Ceram. Ind. 151 (4) (2001) 22–23.
[4] N.P. Padture, M. Gell, E.H. Jordan, Thermal barrier coatings for gas-turbine engine applications, Science 296 (2002) 280–284.
[5] D.R. Clarke, M. Oechsner, N.P. Padture, Thermal-barrier coatings for more efficient gas-turbine engines, MRS Bull. 3 (10) (2012) 891–898.
[6] D. Stover, G. Pracht, H. Lehmann, M. Dietrich, J.E. Doring, R. Vaben, New material concepts for the next generation of plasma-sprayed thermal barrier coatings, in: C. Moreau, B. Marple (Eds.), Thermal Spray 2003: Advancing the Science & Applying the Technology, ASM International, Materials Park, Ohio, USA 2003, pp. 1455–1462.
[7] H. van Esch, J. DeBarro, Coating selection critical to turbine performance, Power Eng. 102 (7) (1998) 44–47.
[8] T.A. Dobbins, R. Knight, M.J. Mayo, HVOF thermal spray deposited Y_2O_3-stabilized ZrO_2 coatings for thermal barrier applications, J. Therm. Spray Technol. 12 (2) (2003) 214–225.
[9] Y. Itoh, M. Saitoh, M. Tamura, Characteristics of MCrAlY coatings sprayed by high velocity oxygen-fuel spraying system, J. Eng. Gas Turbines Power 122 (2000) 43–49.
[10] P. Vuoristo, S. Ahmaniemi, S. Tuurna, T. Mantyla, E. Cordano, F. Fignino, G.C. Gualco, Development of HVOF sprayed NiCoCrAlYRe coatings for use as bond coats of plasma sprayed thermal barrier coatings, Proceedings of ITSC 2002 – International Thermal Spray Conference and Exposition, Essen, Germany, ASM-International/DVS1, 2002, pp. 470–475.
[11] W.O. Soboyejo, P. Mensah, R. Diwan, J. Crowe, S. Akwaboa, High temperature oxidation interfacial growth kinetics in YSZ thermal barrier coatings with bond coatings of NiCoCrAlY with 0,25% Hf, Mater. Sci. Eng. A 528 (2011) 2223–2230.
[12] N. Nayebpashaee, S.H. Seyedein, M.R. Aboutalebi, H. Sarpoolaky, S.M.M. Hadavi, Finite element simulation of residual stress and failure mechanism in plasma sprayed thermal barrier coatings using actual microstructure as the representative volume, Surf. Coat. Technol. 291 (2016) 103–114.
[13] L. Wang, J.S. Yang, J.X. Ni, C.G. Liu, X.H. Zhong, F. Shao, H.Y. Zhao, S.Y. Tao, Y. Wang, Influence of cracks in APS-TBCs on stress around TGO during thermal cycling: a numerical simulation study, Surf. Coat. Technol. 285 (2016) 98–112.
[14] M. Ranjbar-Far, J. Absi, G. Mariaux, Finite element modeling of the different failure mechanisms of a plasma sprayed thermal barrier coatings system, J. Therm. Spray Technol. 21 (6) (2012) 1234–1244.
[15] K. Vaidyanathan, M. Gell, E.H. Jordan, Mechanisms of spallation of electron beam physical vapor deposited thermal barrier coatings with and without platinum aluminide bond coat ridges, Surf. Coat. Technol. 28 (2000) 133–134.
[16] M. Subanovic, P. Song, E. Wessel, R. Vassen, D. Naumenko, L. Singheiser, W.J. Quadakkers, Effect of exposure conditions on the oxidation of MCrAlY-bondcoats and lifetime of thermal barrier coatings, Surf. Coat. Technol. 204 (2009) 820–823.
[17] B.A. Pint, M.A. Bestor, J.A. Haynes, Cyclic oxidation behavior of HVOF bond coatings deposited on La- and Y-doped superalloys, Surf. Coat. Technol. 206 (2011) 1600–1604.
[18] K.G. Schmitt-Thomas, H. Haindl, D. Fu, Modifications of thermal barrier coatings (TBCs), Surf. Coat. Technol. 94–95 (1997) 149–154.
[19] P. Richer, M. Yandouzi, L. Beauvais, B. Jodoin, Oxidation behaviour of CoNiCrAlY bond coats produced by plasma, HVOF and cold gas dynamic spraying, Surf. Coat. Technol. 204 (2010) 3962–3974.
[20] T. Maruyama, M. Yoshiba, K. Kurokawa, Y. Kawahara, N. Otsuka, Characterization of thermally grown oxide on cold sprayed CoNiCrAlY bond coat in thermal barrier coating, Mater. Sci. Forum 696 (2011) 324–329.
[21] A. Manap, A. Nakano, K. Ogawa, The protectiveness of thermally grown oxides on cold sprayed CoNiCrAlY bond coat in thermal barrier coating, J. Therm. Spray Technol. 21 (3) (2012) 586–596.
[22] Q. Chen, W.G. Mao, Y.C. Zhou, et al., Effect of Young's modulus evolution on residual stress measurement of thermal barrier coatings by X-ray diffraction, Appl. Surf. Sci. 256 (23) (2010) 7311–7315.
[23] J. Thornton, S. Slater, J. Almer, The measurement of residual strains within thermal barrier coatings using high-energy X-ray diffraction, J. Am. Ceram. Soc. 88 (10) (2005) 2817–2825.
[24] C.R.C. Lima, J. Nin, J.M. Guilemany, Evaluation of residual stresses of thermal barrier coatings with HVOF thermally sprayed bond coats using the modified layer removal method (MLRM), Surf. Coat. Technol. 200 (20) (2006) 5963–5972.
[25] J. Matějíček, R. Mušálek, P. Chráska, Residual stresses and Young's moduli of plasma sprayed W + Cu composites and FGMs determined by in situ curvature method, Key Eng. Mater. 606 (2014) 151–154.
[26] R.J. Christensen, D.M. Lipkin, D.R. Clarke, K. Murphy, Nondestructive evaluation of the oxidation stresses through thermal barrier coatings using Cr^{3+} piezospectroscopy, Appl. Phys. Lett. 69 (24) (1996) 3754–3756.
[27] E.A.G. Shillington, D.R. Clarke, Spalling failure of a thermal barrier coating associated with aluminum depletion in the bond-coat, Acta Mater. 47 (4) (1999) 1297–1305.
[28] V.K. Tolpygo, D.R. Clarke, K.S. Murphy, Oxidation-induced failure of EB-PVD thermal barrier coatings, Surf. Coat. Technol. 146–147 (2001) 124–131.
[29] K.W. Schlichting, K. Vaidyanathan, Y.H. Sohn, E.H. Jordan, M. Gell, N.P. Padture, Application of Cr3_ photoluminescence piezo-spectroscopy to plasma-sprayed thermal barrier coatings for residual stress measurement, Mater. Sci. Eng. A 291 (2000) 68–77.
[30] D.R. Clarke, R.J. Christensen, V. Tolpygo, The evolution of oxidation stresses in zirconia thermal barrier coated superalloy leading to spalling failure, Surf. Coat. Technol. 94-95 (1997) 89–93.
[31] V. Crespo, I.G. Cano, S. Dosta, J.M. Guilemany, The influence of feedstock powders on the CGS deposition efficiency of bond coats for TBCs, J. Alloys Compd. 622 (2015) 394–401.
[32] A. Rabiei, A.G. Evans, Failure mechanisms associated with the thermally grown oxide in plasma-sprayed thermal barrier coatings, Acta Mater. 48 (2000) 3963–3976.
[33] L. Wang, Y.X. Zhao, X.H. Zhong, S.Y. Tao, W. Zhang, Y. Wang, Influence of island-like oxides in the bond-coat on the stress and failure patterns of the thermal-barrier coatings fabricated by atmospheric plasma spraying during long-term high temperature oxidation, J. Therm. Spray Technol. 23 (3) (2014) 431–446.
[34] M. Martena, D. Botto, P. Fino, S. Sabbadini, M.M. Gola, C. Badini, Modelling of TBC system failure: stress distribution as a function of TGO thickness and thermal expansion mismatch, Eng. Fail. Anal. 13 (2006) 409–426.
[35] M. Caliez, F. Feyel, S. Krunch, J.L. Chaboche, Oxidation induced stress fields in an EB-PVD thermal barrier coating, Surf. Coat. Technol. 157 (2002) 103–110.
[36] A.G. Evans, M.Y. He, J.W. Hutchinson, Mechanics-based scaling laws for the durability of thermal barrier coatings, Prog. Mater. Sci. 46 (2001) 249–271.
[37] H. Hindam, D.P. Whittle, Microstructure, adhesion and growth-kinetics of protective scales on metals and alloys, Oxid. Met. 18 (5–6) (1982) 245–284.
[38] W.R. Chen, X. Wu, B.R. Marple, R.S. Lima, P.C. Patnaik, Pre-oxidation and TGO growth behaviour of an air-plasma-sprayed thermal barrier coating, Surf. Coat. Technol. 202 (2008) 3787–3796.
[39] T. Tomimatsu, S. Zhu, Y. Kagawa, Effect of thermal exposure on stress distribution in TGO layer of EB-PVD TBC, Acta Mater. 51 (2003) 2397–2405.
[40] L.B. Freund, S. Suresh, Thin Film Materials: Stess, Defect Formation and Surface Evolution, Cambridge University Press, Cambridge, UK, 2003.
[41] D.S. Balint, J.W. Hutchinson, An analytical model of rumpling in thermal barrier coatings, J. Mech. Phys. Solids 53 (2005) 949–973.
[42] K.W. Schlichting, N.P. Padture, E.H. Jordan, M. Gell, Failure modes in plasma-sprayed thermal barrier coatings, Mat. Sci. Eng. A 342 (2003) 120–130.
[43] H. Wang, T. Osaki, Y. Nakahara, S. Zhu, Residual stress in oxide on NiCrAlY coating evaluated by photoluminescence spectroscope, Mat. Sci. Forum 750 (2013) 27–30.

Please cite this article as: C.R.C. Lima, et al., Surf. Coat. Technol. (2016), http://dx.doi.org/10.1016/j.surfcoat.2016.07.084